Hadronic Contributions to the Muon $g-2$ in Improved Holographic QCD Models

Jin-Yang Shen(申锦洋)

In collaboration with: Wen-Yuan Peng(彭文苑) 、Ling-Yun Dai(戴凌云)、Zhen Fang(房震)

湖南大学

第五届强子与重味物理理论与实验联合研讨会 · 石家庄

Based mainly on arXiv:2602.23590.

Outline

Muon $g-2$: hadronic contributions and current status

- Muon anomalous magnetic moment:

$$a_\mu = \frac{g_\mu - 2}{2}, \quad a_\mu^{\mathrm{SM}} = a_\mu^{\mathrm{QED}} + a_\mu^{\mathrm{EW}} + a_\mu^{\mathrm{HVP}} + a_\mu^{\mathrm{HLbL}}.$$

- Fermilab precision: 127 ppb (world avg. $\sim$124 ppb)
  [D. P. Aguillard et al., Phys. Rev. Lett. 135, 101802 (2025)]
- With WP2025 lattice LO-HVP input, SM is compatible with experiment.
- **LO-HVP:**
  (1). dominant hadronic uncertainty
  (2). lattice vs data-driven still differ
- **HLbL:**
  (1). subleading but relevant
  (2). dominated by pseudoscalar-pole (π_0, η, and η')
- **Key:** Can holographic QCD provide a unified description of HVP and HLbL simultaneously?

[WP2025 update: R. Aliberti et al., Phys. Rept. 1143, 1 (2025)]

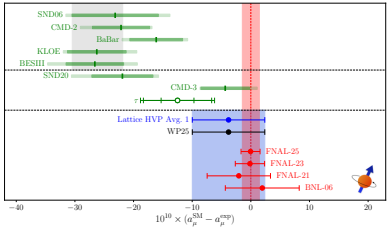

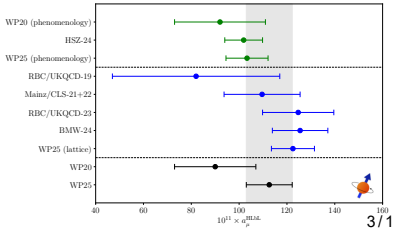

Historical background: holographic $g-2$ program

- 2009–2011: first AdS/QCD constructions for HVP/HLbL in Hard-Wall model.
  D. K. Hong et al., Phys. Rev. D 81, 073005 (2010); L. Cappiello et al., Phys. Rev. D 83, 093006 (2011).
- 2019–2020: pseudoscalar-pole and axial-vector HLbL contributions.
  J. Leutgeb et al., Phys. Rev. D 100, 094038 (2019); J. Leutgeb et al., Phys. Rev. D 101, 114015 (2020).
- 2022: dedicated LO-HVP benchmark in minimal holographic models.
  J. Leutgeb et al., Phys. Rev. D 105, 094032 (2022).
- 2023–2025: extensions to axial-vector / tensor channels and short-distance constraints.
  P. Colangelo et al., Phys. Rev. D 109, 094036 (2024); J. Mager et al., Phys. Rev. Lett. 135, 091901 (2025).
- These works are all based on the standard hard-wall and soft-wall models, both of which suffer from certain shortcomings.

Hard-wall vs Soft-wall

Common setup

- AdS$_5$: $ds^2 = z^{-2}(\eta_{\mu\nu}dx^\mu dx^\nu - dz^2)$, where $\eta_{\mu\nu} = (1,-1,-1,-1)$.
- 5D gauge fields $A^{(L,R)}$ + scalar X.
- UV matching: $g_5^2 = 12\pi^2/N_c$.

Hard-wall (HW)

$$S = \int d^5x\,\sqrt{g}\,\mathrm{Tr}[|DX|^2 + m_5^2|X|^2 - \frac{1}{4g_5^2}(F_L^2+F_R^2)]$$

- Sharp IR cutoff at $z = z_0$.
- Simpler structure, but less smooth IR dynamics.

[J. Erlich et al., Phys. Rev. Lett. 95, 261602 (2005)]

Soft-wall (SW)

$$S = \int d^5x\,\sqrt{g}\,e^{-\Phi(z)}\,\mathrm{Tr}[|DX|^2 + m_5^2|X|^2 - \frac{1}{4g_5^2}(F_L^2+F_R^2)]$$

- Smooth IR via dilaton profile $\Phi(z) = \kappa^2 z^2$.
- Naturally supports Regge-like $m_n^2 \sim n$.

[H.R. Grigoryan et al., Phys. Rev. D 76, 095007 (2007)]

In this work

- Adopt IR-improved soft-wall models (SW1/SW2/SW3). These variants are designed to test how IR modeling and chiral dynamics affect precision observables.cc
- Test predictive power with spectroscopy, HVP and HLbL-related observables.

SW1/SW2/SW3 models

- For SW1 and SW2 models, the common $N_f = 2$ bulk action:

$$S_{N_f=2} = \int d^5x \sqrt{g}\, e^{-\Phi(z)} \mathrm{Tr}\Big[|DX|^2 - m_5^2(z)|X|^2 - \lambda_X|X|^4 - \frac{1}{4g_5^2}\left(F_L^2 + F_R^2\right)\Big].$$

- SW3 extends to $N_f = 2 + 1$ with an additional flavor-mixing term:$\gamma\,\mathrm{Re}\{\det X\}$
- Physics of γ: it couples light and strange chiral dynamics and is essential for realistic 2+1 flavor behavior.
- Key strategy: fix one common action backbone and isolate differences from IR modeling.

[L.-X. Cui et al., Eur. Phys. J. C 76, 22 (2016);Z. Fang et al., Phys. Lett. B 762, 86 (2016); Z. Fang et al., Phys. Rev. D 100, 054008 (2019)]

Model Difference I

- Dilaton profiles in the three models:

$$\Phi_{\mathrm{SW1}}(z) = \mu_g^2 z^2 - \frac{\lambda_g^4 \mu_g^4 z^4}{(1+\mu_g^2 z^2)^3}, \quad \Phi_{\mathrm{SW2}}(z) = \mu_g^2 z^2, \quad \Phi_{\mathrm{SW3}}(z) = \mu_g^2 z^2 \left(1 - e^{-\mu_g^2 z^2/4}\right).$$

- Shared target: approximately quadratic IR growth for Regge-like trajectories, while keeping near-conformal UV behavior.
- SW2/SW3 use a running scalar bulk mass:

$$m_5^2(z) = -3 - \mu_c^2 z^2,$$

  improving consistency between confinement and chiral symmetry breaking.
- Main point: the first SW1/2/3 separation comes from the background choice, which then propagates to vector correlators and TFFs.

Model Difference II

SW1 ($N_f = 2$): analytic ansatz fixed by UV/IR asymptotics

$$\chi(z) = \frac{Az + Bz^3}{1 + Cz^2}$$

SW2 ($N_f = 2$): solve χ directly from the EOM with boundary $\chi'(0) = m_u\zeta$ (more dynamical)

$$\chi'' - \left(\frac{3}{z} + \Phi'\right)\chi' - \frac{1}{z^2}\left(m_5^2(z)\chi + \frac{\lambda}{2}\chi^3\right) = 0$$

SW3 ($N_f = 2 + 1$): coupled light–strange system with γ-mixing

$$\langle X \rangle = \frac{1}{\sqrt{2}}\mathrm{diag}(\chi_u, \chi_u, \chi_s)$$

Takeaway: Different χ constructions drive different chiral dynamics.

Step 1: Validate Spectroscopy Before Computing $g-2$

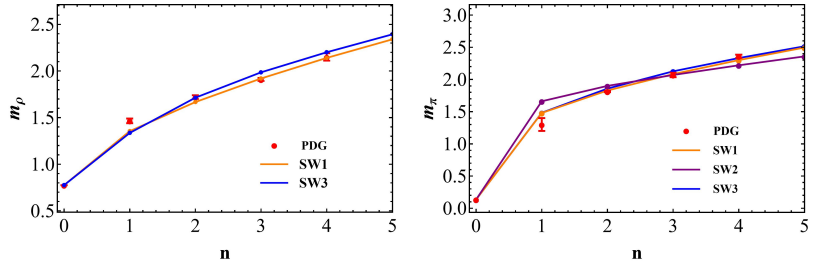

- Workflow: validate masses and decay constants first, then compute $\Pi_V(Q^2)$ and TFFs.
- SW1/SW3 generally perform better than SW2; vector decay constants are the sharpest discriminator.

Model	SW1	SW2	SW3	Exp.
$F_\rho^{1/2}$ [MeV]	329.4	260.0	308.0	~ 348
f_π [MeV]	92.4	92.4	92.4	92.4

Step 2: electromagnetic correlator as a model test

- Physics question: can the same validated hadron model reproduce the vector-current correlator entering HVP?
- LO-HVP is obtained from the Euclidean vacuum-polarization integral

$$a_\mu^{\mathrm{LO-HVP}} = 4\pi^2 \left(\frac{\alpha}{\pi}\right)^2 \int_0^\infty dQ^2\, f(Q^2)\, \hat{\Pi}_{\mathrm{em}}^{\mathrm{had}}(Q^2).$$

- $f(Q^2)$ strongly enhances low-Q^2; thus low-energy vector dynamics is decisive.
- In this setup, $\hat{\Pi}_{\mathrm{em}}^{\mathrm{had}}$ is built from holographic Π_V^{ren}.
- For $N_f = 2$: $\hat{\Pi}_{\mathrm{em}}^{\mathrm{had}} = \frac{10}{9}\Pi_V^{ren}$.
- SW2: analytic correlator; SW1/SW3: resonance-sum reconstruction:

$$\Pi_V^{\mathrm{ren}}(-q^2) = \sum_{n=1}^{I} \frac{q^2 F_{\rho^n}^2}{(q^2 - m_{\rho^n}^2)\, m_{\rho^n}^4} + \mathcal{O}\left(\frac{q^2}{m_{\rho^{I+1}}^2}\right)$$

LO-HVP results: what is learned about the models?

Model	$a_\mu^{\mathrm{LO-HVP}} \times 10^{10}$
SW1	482.5
SW2	276.4
SW3	404.0
HW	476.9
Original SW	276.4

- Ordering is stable: SW1 $>$ SW3 $>$ SW2.
- Baseline values are below the dispersive sum of the selected 2π, 3π and $\pi_0\gamma$ channels, approximately 557×10^{-10}. J. Leutgeb et al., Phys. Rev. D 105, 094032 (2022).
- Interpretation: improved IR modeling helps, but vector strength normalization remains the bottleneck.
- This deficit is strongly correlated with the underestimation of vector decay constants.

HVP interpretation: beyond numbers

- The gap to dispersive estimates is not random: it tracks F_ρ in the vector channel.
- This identifies a concrete model-building target: improve vector decay constants while preserving spectra/TFF quality.
- A tuned SW1 with physical m_ρ and F_ρ gives

$$a_\mu^{\mathrm{LO-HVP}} \approx 573.5 \times 10^{-10}.$$

- So HVP here is used as a diagnostic of model consistency, not just a final number.

Takeaway

HVP quantitatively tests whether holographic vector dynamics is realistic enough for precision phenomenology.

Pion transition form factor in holography

- The HLbL pseudoscalar-pole contribution is controlled by $F_{\pi^0\gamma^*\gamma^*}(Q_1^2, Q_2^2)$.
- Flavor anomalies follow uniquely from the 5D Chern-Simons term:

$$S_{\text{CS}} = \frac{N_c}{24\pi^2}\int \text{tr}\left(AF^2 - \frac{i}{2}A^3F - \frac{1}{10}A^5\right)\Big|_{L-R}.$$

- The pion transition form factor then takes the form:

$$F_{\pi^0\gamma^*\gamma^*}(Q_1^2, Q_2^2) = -\frac{N_c}{12\pi^2}K(Q_1^2, Q_2^2),$$

$$K = -\int_0^\infty V(Q_1, z)V(Q_2, z)\partial_z\varphi(z)\, dz.$$

- $V(Q, z)$: photon bulk propagator; $\varphi(z)$: pion profile.
- Anomaly normalization at $Q_1^2 = Q_2^2 = 0$ is recovered: $F_{\pi_0\gamma\gamma} = \frac{N_c}{12\pi^2 f_\pi}$.

Ground-state pion wave functions

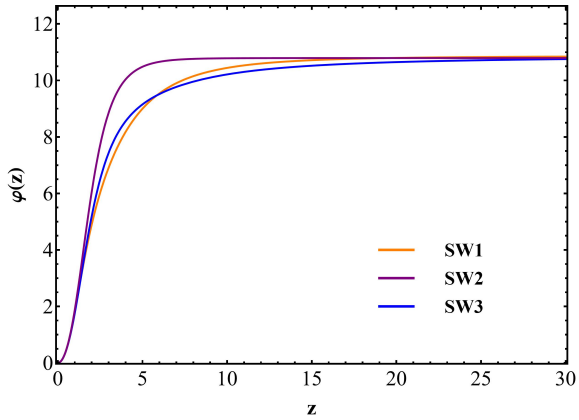

- Differences appear at small z.
- Profiles approach a common asymptotic limit $1/f_\pi$ at larger z.

TFF at intermediate/high momentum

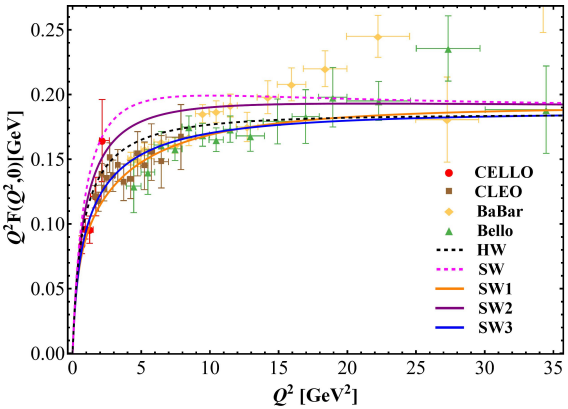

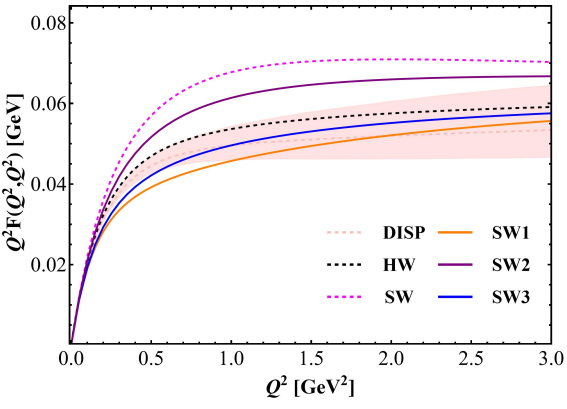

Left: $Q^2F(Q^2,0)$ Right: $Q^2F(Q^2,Q^2)$

- Correct asymptotic trend: $Q^2F(Q^2,0) \to 2f_\pi$.
- SW1/SW3 are closer to the dispersive diagonal band.

[HW: J. Erlich et al., Phys. Rev. Lett. 95, 261602 (2005);SW: P. Colangelo et al., Phys. Lett. B 840, 137878(2023)]

Three-dimensional TFF surfaces

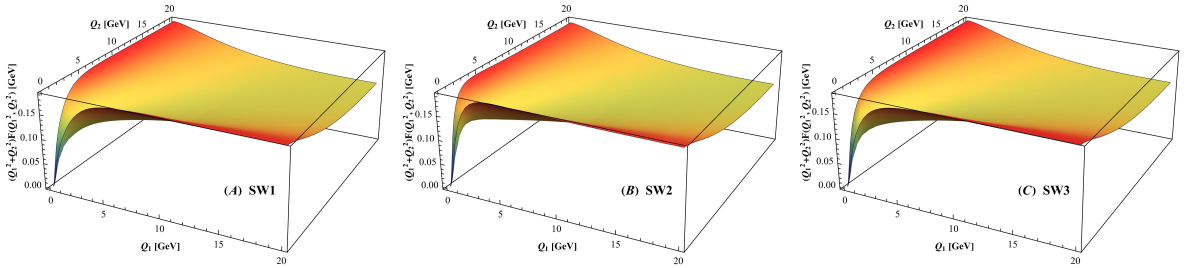

- Gives a global view of model-dependent (Q_1^2, Q_2^2) behavior.
- Useful for discussing UV stability and interpolation quality.

HLbL pole results: second independent validation

- Insert holographic TFF into the standard HLbL integral.

Model / Reference	$a_\mu^{\pi^0} \times 10^{11}$
SW1	56.1
SW2	68.6
SW3	58.7
HW	65.2
SW	75.2
White Paper 2025	$63.6^{+3.0}_{-2.5}$
BMW lattice	$57.8 \pm 1.8 \pm 0.9$

- TFF low-Q^2 behavior? pion wavefunction difference?

Summary

- Improved soft-wall holographic QCD provides a realistic framework for hadronic contributions to $(g-2)_\mu$.
- HVP probes vector-current realism, while HLbL probes transition-form-factor realism.
- Precision observables such as HVP and HLbL provide stronger model discrimination than hadron spectra alone.
- A more complete HLbL description requires the inclusion of axial-vector, tensor, and higher-excited-state contributions.

Thank you very much for your patience!